Observations of tidal variability on the New England shelf

R. Kipp Shearman and Steven J. Lentz

Department of Physical Oceanography, Woods Hole Oceanographic Institution, Woods Hole, Massachusetts, USA

Received 20 May 2003; revised 19 November 2003; accepted 31 December 2003; published 4 June 2004.

[1] Observations from the Coastal Mixing and Optics experiment moored array, deployed from August 1996 through June 1997, are used to describe barotropic and baroclinic tidal variability over the New England shelf. The dominant M_2 tidal elevations decrease toward the northeast to a minimum over the Nantucket shoals (about 34 cm), and barotropic tidal current amplitudes increase strongly toward the northeast to a maximum over the shoals (about 35 cm s^{-1}). Estimates of the depth-averaged M_2 momentum balance indicate that tidal dynamics are linear, and along-shelf pressure gradients are as large as cross-shelf pressure gradients. In addition, tidal current ellipses are weakly polarized, confirming that the dynamics are more complex than simple plane waves. The vertical structure of the M_2 currents decreases in amplitude and phase (phase lead near bottom) over the bottom 20 m. The M_2 momentum deficit near the bottom approximately matches direct covariance estimates of stress, confirming the effects of stress on current structure in the tidally driven bottom boundary layer. Baroclinic current variability at tidal frequencies is small (2 cm s^{-1} amplitude), with a predominantly mode 1 vertical structure. High-frequency (approaching the buoyancy frequency) internal solitons are observed following the pycnocline. The internal solitons switch from waves of depression to waves of elevation when the depth of maximum stratification is deeper than half the water column depth. Both low-mode baroclinic tidal and high-frequency internal wave energy decrease linearly with bottom depth across the shelf. *INDEX TERMS:* 4219 Oceanography: General: Continental shelf processes; 4223 Oceanography: General: Descriptive and regional oceanography; 4544 Oceanography: Physical: Internal and inertial waves; 4560 Oceanography: Physical: Surface waves and tides (1255); *KEYWORDS:* continental shelf, barotropic tides, baroclinic tides

Citation: Shearman, R. K., and S. J. Lentz (2004), Observations of tidal variability on the New England shelf, *J. Geophys. Res.*, *109*, C06010, doi:10.1029/2003JC001972.

1. Introduction

[2] Barotropic and baroclinic tides are a common and often large component of current variability over the continental shelf. Along the Middle Atlantic Bight (MAB) and over the New England shelf, the barotropic tide has received considerable attention [*Beardsley et al.*, 1977; *Moody et al.*, 1983; *Daifuku and Beardsley*, 1983; *Brown*, 1984; *Lentz et al.*, 2001]. However, much about tidal dynamics over the New England shelf remains ambiguous [*Brown*, 1984]. In addition, internal waves at tidal frequencies are observed on the New England shelf, as well as high-frequency (approaching N, the buoyancy frequency) internal solitons [e.g., *Colosi et al.*, 2001] generated at intervals related to the barotropic tide. The magnitude, phase and structure of baroclinic tides are potentially highly variable, depending on forcing mechanisms (such as the barotropic tide) and the presence, strength, and structure of stratification. The New England shelf undergoes a large seasonal change in stratification [*Beardsley et al.*, 1985], and the presence and movement of the shelf slope front [*Houghton et al.*, 1988; *Linder and Gawarkiewicz*, 1998] combine to create variations in the density field over a range of spatial and temporal scales [e.g., *Linder and Gawarkiewicz*, 1998; *Lentz et al.*, 2003]. It is unknown how this variability affects tidal current variability on the New England shelf.

[3] Barotropic and baroclinic tides are important because they affect a variety of shelf processes including bottom stress and frictional dissipation, property mixing in the bottom boundary layer, and sediment resuspension. Also, barotropic and baroclinic tidal variability are a source of noise for ship-based synoptic hydrographic and current surveys [e.g., *Gawarkiewicz et al.*, 2004]. Thus having a detailed description and understanding of the processes that affect the structure and temporal variability of tides is a valuable goal.

[4] Data from a densely instrumented moored array (Figure 1), deployed as part of the Office of Naval Research sponsored Coastal Mixing and Optics (CMO) experiment [*Dickey and Williams*, 2001], are used here to describe the magnitude, three-dimensional structure, temporal variability and dynamics of barotropic and baroclinic tidal fluctuations over the New England shelf. Also, moored current observations from the 1979–1980 Nantucket Shoals Flux Experiment (NSFE) [*Beardsley et al.*, 1985], the 1983–1984 Shelf Edge Exchange Processes study (SEEP) [*Aikman et al.*, 1988], the 1995–1997 Shelfbreak Primer

0148-0227/04/2003JC001972$09.00

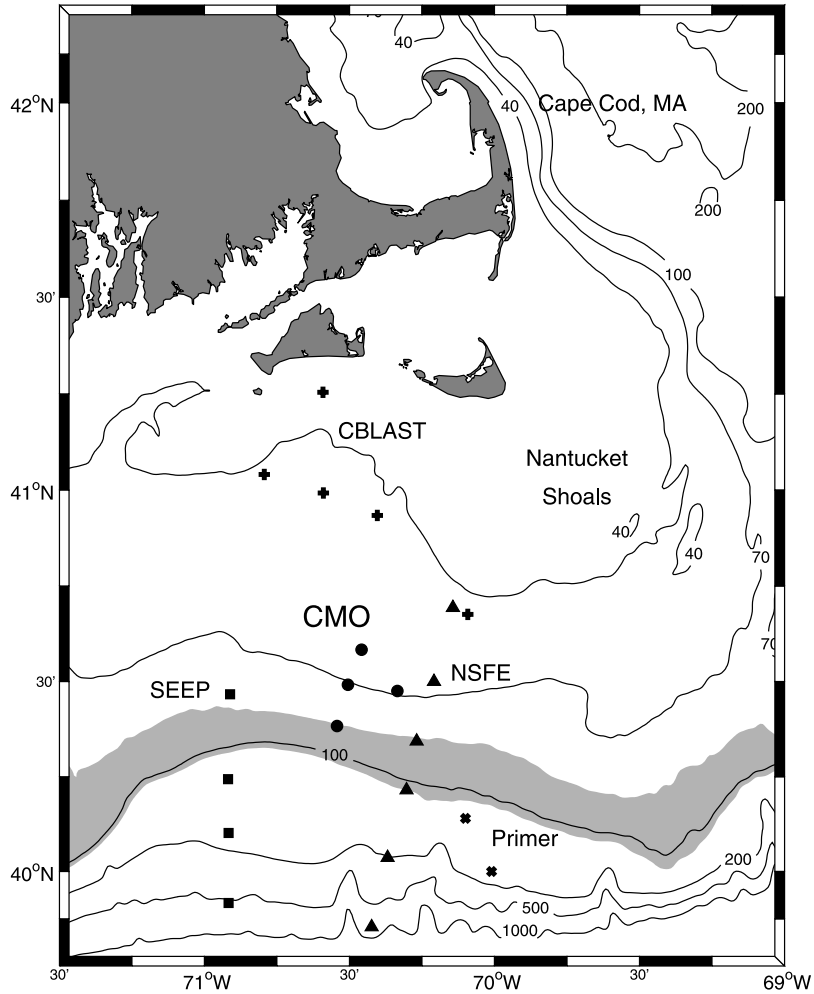

Figure 1. Location of the Coastal Mixing and Optics (CMO) experiment moored array and bathymetry over the New England shelf. Also shown are the Nantucket Shoals Flux Experiment (NSFE), Shelf Edge Exchange Processes (SEEP) study, Coupled Boundary Layers Air-Sea Transfer (CBLAST) experiment, and Shelfbreak Primer mooring sites.

program [*Fratantoni and Pickart*, 2003], and the 2001 Coupled Boundary Layers Air-Sea Transfer (CBLAST) experiment are used to place the CMO observations in a broader context. The CMO moored array observations present the opportunity to expand our understanding of the characteristics of tidal variability over the New England shelf. Specifically, the concomitant high vertical resolution measurements of current, temperature, conductivity and near-bottom stress [*Shaw et al.*, 2001] are unique for this region.

[5] The remainder of this paper is organized as follows. Section 2 describes the CMO moored array observations and the principal methods used to analyze the data. Section 3 examines barotropic tidal variability. Section 4 examines baroclinic variability associated with tides, including the internal tide and high-frequency internal solitons whose generation is associated with the tide. Finally, section 5 discusses and summarizes the preceding material.

2. CMO Moored Array

[6] The CMO moored array was deployed on the New England shelf ~100 km south of Cape Cod, Massachusetts (Figure 1). This region of the New England shelf is oriented roughly east-west and relatively broad (about 100 km wide), although the distance from the 40 m isobath to the shelfbreak (approximately the 150 m isobath) narrows to the east due to the presence of the Nantucket shoals. The CMO moored array consisted of four sites, occupied continuously from August 1996 through June 1997. The central site was located at 40°29.5′N, 70°30.5′W in 70 m of water, and the three surrounding sites (inshore, offshore and alongshore) were located ~11 km inshore in 64 m of water, 12.5 km offshore in 86 m of water, and 14.5 km east along the 70 m isobath. All four sites included observations of currents, temperature and conductivity spanning the water column (Figure 2). Bottom pressure was measured at the inshore, offshore and alongshore sites. Also at the central site, near-bottom currents and direct covariance estimates of near-bottom stress were made using acoustic travel time velocimeters mounted on a Benthic Acoustic Stress Sensor (BASS) tripod [*Williams et al.*, 1987]. There were three BASS deployments over the course of the CMO experiment: 18 August to 27 September 1996; 7 October to 16 November 1996; and 17 April to 10 June 1997 [*Shaw et al.*, 2001].

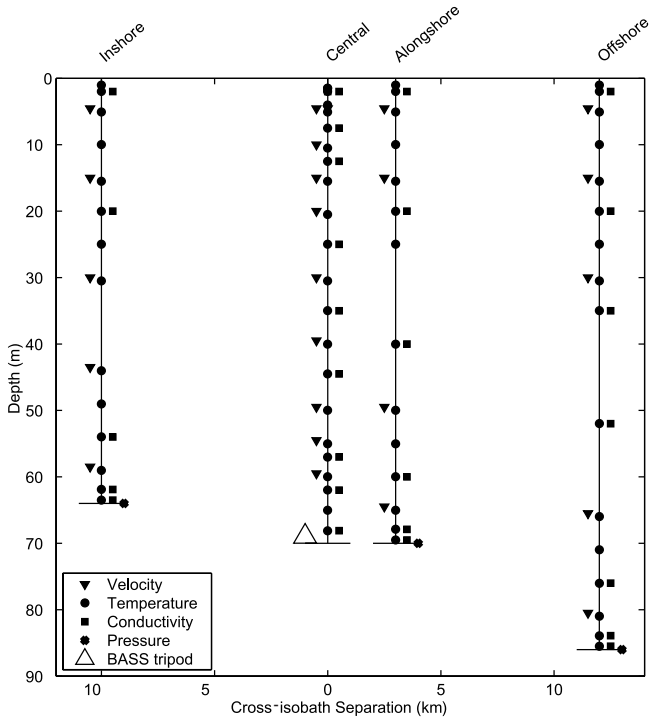

Figure 2. Subsurface instrumentation on the CMO moored array.

[7] A thorough description of the moored instrumentation, sampling strategies, and data processing techniques is presented by *Galbraith et al.* [1999]. Bottom pressure was measured using SeaBird Seagauge pressure sensors with a 5 min sample interval. Sea level was estimated from the bottom pressure (P^b) and density (ρ) observations:

$$\eta = \frac{P^b}{g\rho_0} - \int_{-h}^{0} \frac{\rho}{\rho_0} dz, \quad (1)$$

where $\rho_0 = 1025$ kg m^{-3} is the constant volume-averaged density, $g = 9.81$ m s^{-2} is the gravitational acceleration and h is the bottom depth. Vector-measuring current meters (VMCMs) were used to measure currents with a 7.5 min sample interval. Time series of the raw observations were low-pass filtered to remove variability at timescales less than one hour, and then decimated to hourly values. The accuracy of hourly current observations is estimated to be 2–3 cm s^{-1} [*Beardsley*, 1987], and the precision of sea level estimates from bottom pressure is about 1 cm.

[8] Near-bottom stress and current vectors are analyzed in an along-isobath and cross-isobath coordinate frame, where the positive x axis (along-isobath direction) is oriented toward 110 T and the positive y axis (cross-isobath direction) is oriented toward 20 T. This orientation is estimated from the bathymetry over length scales of 10–50 km, and the along-isobath direction matches the orientation of the principal axes of the depth-averaged subtidal flow [*Shearman and Lentz*, 2003]. Depth-averaged currents at each site are estimated from the VMCM observations, using a trapezoidal integration scheme and assuming constant velocity between the shallowest (deepest) observation and the surface (bottom).

[9] Tidal amplitude and phase are estimated using harmonic analysis [*Foreman*, 1977, 1978; *Pawlowicz et al.*, 2002], following applications by *Beardsley et al.* [1995] and *Lentz et al.* [2001]. All sea level, depth-averaged current and most current meter records are 310 days long. There are short (~10 day) gaps at two inshore site current meters (15 and 30 m), and three current meters (inshore 4.6 m, alongshore 4.6 and 15 m) with substantially shorter records were excluded from individual tidal analyses. Uncertainties (95% confidence intervals) for tidal current ellipse parameters are estimated [*Beardsley et al.*, 1995; *Lentz et al.*, 2001]. Tidal constituents are also fit to the BASS tripod current observations. The BASS current records have two large time gaps between the three deployments. Tidal fits to the moored current data do not differ significantly using the full moored current meter time series or the subset that matches the BASS current time series. Finally, detided current observations are estimated by removing the significant (signal-to-noise ratio greater than 2) tidal constituents given by the full record harmonic analysis at each instrument. The same tidal analysis procedure is applied to the NSFE, SEEP, Primer and CBLAST data.

3. Barotropic Tidal Variability

[10] Although the New England shelf is described as a region of minimum tidal amplitude [*Moody et al.*, 1983; *Brown*, 1984], the diurnal and semidiurnal tidal current and sea level variances during CMO are still a large fraction of the total variance. At the inshore site (the other sites are qualitatively similar), spectra of sea level and depth-averaged currents are dominated by large, narrow-banded peaks at the principal diurnal (K_1, O_1, P_1) and semidiurnal (M_2, N_2, S_2) constituent frequencies with the M_2 being the largest by nearly an order of magnitude (Figure 3). For currents, clockwise rotary spectra are much larger than the counterclockwise spectra. At the inshore site, diurnal (0.85–1.05 cpd) and semidiurnal (1.80–2.10 cpd) band variance account for 43% and 69% of the total depth-averaged along- and cross-isobath current variance and 96% of the total sea level variance (timescales ranging from 2 hours to 10 months). In addition, there are significant peaks in both sea level and depth-averaged currents at the higher tidal harmonic frequencies.

[11] The six principal sea level tidal constituents, estimated by harmonic analysis, in order of magnitude are the M_2, N_2, S_2, K_1, O_1, and P_1 (Table 1). The M_2 amplitude (about 41 cm) is ~4 times larger than the next largest constituent. Sea level amplitude and phase for each constituent are nearly constant across the CMO array (~20 km separation), varying by less than 1 cm and 3°G. The M_2 and K_1 are the largest depth-averaged current tidal constituents (Table 1), followed by the N_2 and O_1, which are similar in magnitude, and finally the S_2 and P_1. The M_2 major axes (between 8–13 cm s^{-1}) are 2–3 times larger than the K_1 major axes. The major axes of almost all constituents increase in the on-shelf and eastward along-shelf directions. Phase and ellipse orientation for each constituent are approximately constant (within error estimates) over the CMO array. All the major constituent vectors rotate clockwise, and depth-averaged tidal ellipses are roughly circular with ellipticities (ratio of minor to major axes)

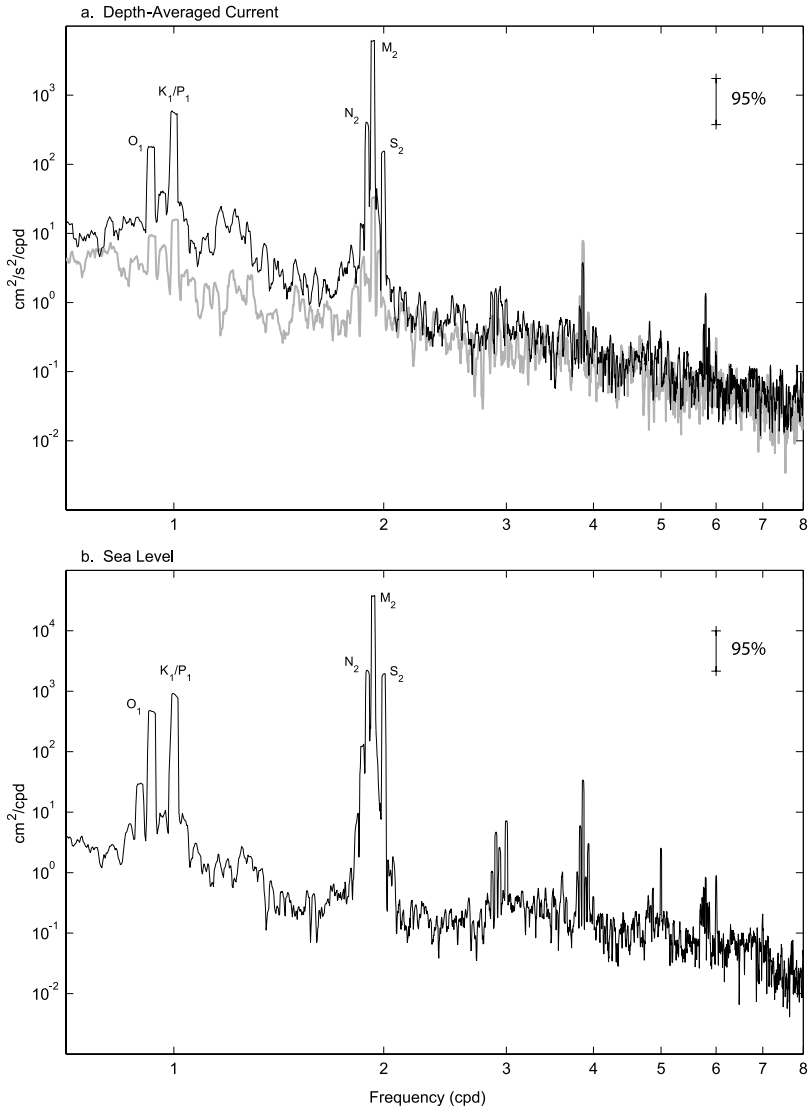

Figure 3. (a) Rotary current spectra (black line, clockwise; gray line, counterclockwise) for the depth-averaged current and (b) spectrum of sea level variations (estimated from bottom pressure) at the inshore site. Individual peaks at tidal constituent frequencies are labeled.

ranging from -0.7 to -1.0. The CMO estimates of tidal phase and amplitude are consistent with previous estimates in the same region [i.e., *Moody et al.*, 1983].

[12] The dynamics of the dominant M_2 tidal constituent are examined through harmonic analysis of the terms in the depth-averaged horizontal momentum balance:

$$-i\omega\langle\mathbf{u}\rangle + \langle\mathbf{u}\cdot\nabla\mathbf{u}\rangle + f\hat{k}\times\langle\mathbf{u}\rangle = -\langle\nabla P/\rho_0\rangle - \frac{\tau^b}{h\rho_0}, \qquad (2)$$

where ∇ is the horizontal gradient operator, $\omega = 1.41 \times 10^{-4}$ s^{-1} is the M_2 tidal constituent frequency, $f = 0.94 \times 10^{-4}$ s^{-1} is the local Coriolis parameter, and $\langle\ \rangle$ indicate a depth average. The terms of the horizontal momentum budget are estimated from the CMO moored array observations of current, bottom stress, bottom pressure and density. Horizontal pressure and velocity gradients are estimated, using a sigma (z/h) vertical coordinate, by fitting a plane to the observations at a sigma level across the CMO array then correcting for the slope of the sigma level to convert back to x, y, z coordinates [see *Shearman and Lentz*, 2003]. Current observations are spatially averaged to match the scale of the pressure gradient estimates. In both the along- and cross-isobath balances, the local acceleration term is largest, followed by Coriolis and the pressure gradient (Table 2). The nonlinear terms and bottom stress are very small (more than an order of magnitude less). Tidal analysis of the residual, the difference between the left and right hand sides of equation (2), is also very small, suggesting all dynamically important terms have been accurately estimated. In both the along- and cross-isobath directions, the local acceleration term is approximately balanced by Coriolis and the pressure gradient. The pressure gradient term is highly barotropic; that is, results of harmonic analysis using only the sea level gradient are nearly identical to the depth average of the total pressure gradient.

[13] A similar distribution of momentum was found by *Brown* [1984]. Dynamically, the M_2 tide over the New

Table 1. Sea Level Amplitude and Phase and Depth-Averaged Current Ellipse Parameters (Major Axis, Minor Axis, Orientation, and Phase) for the Six Largest Tidal Constituents, Estimated via Harmonic Analysis[a]

Constituent	Sea Level		Depth-Averaged Current			
Name	Amplitude, cm	Phase, °G	Major Axis, cm s^{-1}	Minor Axis, cm s^{-1}	Ellipse Orientation, °T	Phase, °G
			Inshore			
M2	41.1 ± 0.1	352.0 ± 0.2	12.5 ± 0.2	−10.9 ± 0.1	33.3 ± 3.7	45.6 ± 3.6
N2	9.8 ± 0.1	334.8 ± 0.8	3.1 ± 0.2	−2.8 ± 0.1	69.6 ± 21.6	336.5 ± 21.1
S2	9.2 ± 0.1	17.2 ± 0.9	1.9 ± 0.2	−1.7 ± 0.2	168.7 ± 36.7	280.4 ± 36.5
K1	7.1 ± 0.2	173.2 ± 1.6	4.8 ± 0.6	−3.5 ± 0.4	174.1 ± 14.6	6.9 ± 16.6
O1	5.2 ± 0.2	184.2 ± 2.4	2.9 ± 0.6	−1.9 ± 0.4	174.7 ± 18.3	330.0 ± 22.0
P1	2.4 ± 0.2	175.2 ± 4.2	1.1 ± 0.4	−1.1 ± 0.4	86.1 ± 138.8	96.0 ± 131.4
			Central			
M2			11.0 ± 0.2	−9.7 ± 0.2	35.9 ± 5.1	45.2 ± 5.1
N2			2.9 ± 0.2	−2.6 ± 0.2	74.8 ± 23.2	332.6 ± 23.3
S2			1.6 ± 0.2	−1.4 ± 0.2	174.8 ± 46.2	276.2 ± 44.8
K1			4.8 ± 0.5	−3.7 ± 0.4	175.7 ± 16.1	8.7 ± 17.5
O1			2.7 ± 0.6	−2.2 ± 0.5	172.9 ± 40.1	333.2 ± 44.1
P1			1.3 ± 0.4	−1.1 ± 0.4	159.5 ± 93.7	24.4 ± 88.4
			Offshore			
M2	42.0 ± 0.1	350.3 ± 0.2	8.1 ± 0.2	−7.2 ± 0.2	34.1 ± 7.9	46.0 ± 8.3
N2	9.8 ± 0.1	332.5 ± 0.8	2.1 ± 0.2	−2.0 ± 0.2	88.4 ± 58.3	318.7 ± 58.5
S2	9.2 ± 0.1	16.0 ± 0.8	1.2 ± 0.2	−1.0 ± 0.2	150.4 ± 29.6	299.3 ± 29.6
K1	7.6 ± 0.1	174.3 ± 1.2	4.1 ± 0.5	−2.8 ± 0.4	2.7 ± 15.1	187.8 ± 16.1
O1	5.5 ± 0.1	182.6 ± 1.8	2.6 ± 0.6	−2.0 ± 0.5	0.4 ± 40.3	155.0 ± 44.5
P1	2.5 ± 0.1	175.3 ± 3.1	1.1 ± 0.5	−0.8 ± 0.4	5.1 ± 67.0	190.2 ± 75.7
			Alongshore			
M2	40.8 ± 0.1	351.4 ± 0.2	12.7 ± 0.3	−10.5 ± 0.3	26.6 ± 4.5	45.8 ± 4.7
N2	9.7 ± 0.1	334.1 ± 0.7	2.9 ± 0.2	−2.7 ± 0.2	63.8 ± 53.0	332.2 ± 52.5
S2	9.1 ± 0.1	17.2 ± 0.8	1.9 ± 0.3	−1.6 ± 0.3	149.3 ± 36.6	293.6 ± 39.4
K1	7.3 ± 0.2	173.7 ± 1.4	4.8 ± 0.7	−3.5 ± 0.5	171.6 ± 19.7	13.7 ± 19.8
O1	5.4 ± 0.2	182.9 ± 2.1	3.0 ± 0.7	−2.3 ± 0.5	2.4 ± 43.7	146.3 ± 45.3
P1	2.4 ± 0.2	175.7 ± 3.7	1.1 ± 0.6	−0.7 ± 0.4	164.4 ± 56.9	359.4 ± 65.2

[a]The 95% confidence intervals are indicated. Minor axes less than zero indicate clockwise rotation of the tidal current vector.

England shelf is unlike either of the regions immediately to the west (New Jersey Shelf) or east (Gulf of Maine and Georges Bank), where simple models adequately reproduce tidal currents and elevations [e.g., *Clarke*, 1991; *Brown*, 1984]. Although the cross-isobath balance is similar to that over central Georges Bank, the along-isobath balance is different due to the importance of the along-isobath pressure gradient (which is negligible over Georges Bank). The affect of the along-isobath pressure gradient is evident in the ellipticity of depth-averaged M_2 tidal currents (about 0.90), which is significantly different than the ellipticity predicted by a simple plane wave solution ($f/\omega = 0.67$). The implication is that the M_2 tide on the New England shelf is more complicated than a simple standing or progressive planar wave.

[14] The source of the along-isobath pressure gradient is potentially related to the bathymetric irregularity caused by the Nantucket shoals, which is the location of a strong local minimum in M_2 tidal elevation and maximum in tidal currents. Larger-scale maps of the tidal characteristics [*Moody et al.*, 1983; *Brown*, 1984] indicate that the New England shelf south of Cape Cod is a transition region between the dynamically distinct MAB shelf to the west and the resonant Gulf of Maine to the northeast. The detailed importance of the local bathymetry and the potentially enhanced drag over the Nantucket shoals to the tidal characteristics in this transition region are unclear (the addition of an along-isobath propagating or standing wave is one possibility) and beyond the scope of this particular effort, but there is clear motivation for a modeling study

Table 2. Amplitude (A) and Phase (ϕ) for Terms in the Depth-Averaged M_2 Along- and Cross-Isobath Momentum Balances and Residuals[a]

	Local Acceleration	Nonlinear 1	Nonlinear 2	Coriolis	Pressure Gradient	Bottom Stress	Residual
	$-i\omega\langle u\rangle/f$	$\langle uu_x\rangle/f$	$\langle vu_y\rangle/f$	$-\langle v\rangle$	$\langle P_x/f\rho_0\rangle$	$\tau^{bx}/hf\rho_0$	R^x
A^x, cm s^{-1}	15.39 ± 0.24	0.19 ± 0.08	0.18 ± 0.07	10.80 ± 0.16	5.17 ± 0.20	0.17 ± 0.01	0.15 ± 0.24
ϕ^x, °G	6 ± 1	252 ± 23	2 ± 24	194 ± 1	170 ± 2	82 ± 5	213 ± 113
	$-i\omega\langle v\rangle/f$	$\langle uv_x\rangle/f$	$\langle vv_y\rangle/f$	$\langle u\rangle$	$\langle P_y/f\rho_0\rangle$	$\tau^{by}/hf\rho_0$	R^y
A^y, cm s^{-1}	16.04 ± 0.28	0.12 ± 0.06	0.03 ± 0.03	9.63 ± 0.12	6.95 ± 0.16	0.15 ± 0.01	0.48 ± 0.27
ϕ^y, °G	284 ± 1	130 ± 27	10 ± 76	97 ± 1	116 ± 1	5 ± 5	129 ± 34

[a]The 95% confidence intervals from the harmonic analysis are included.

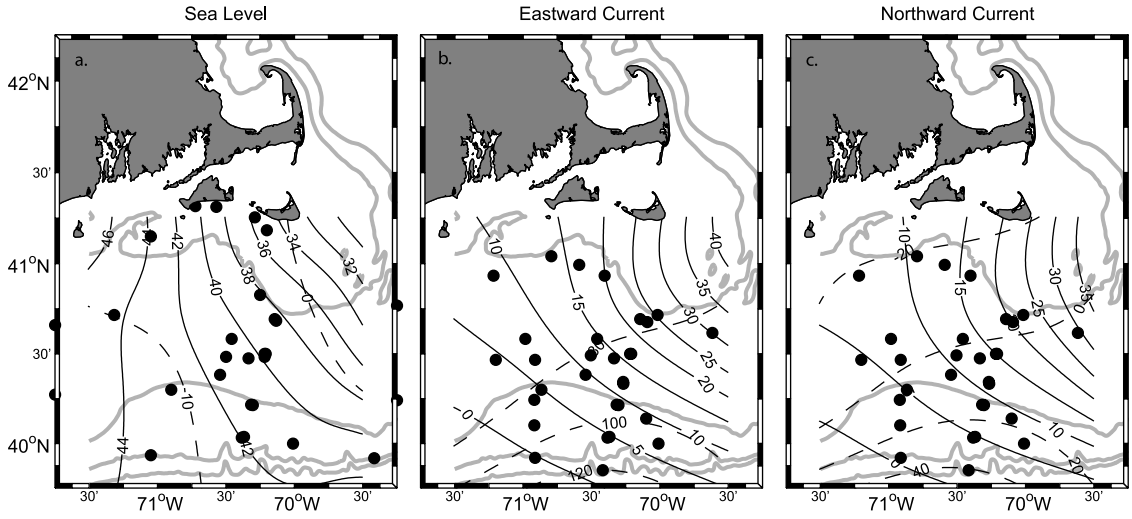

Figure 4. Maps of M_2 amplitude (solid line) and phase (dashed line) over the New England shelf for (a) sea level elevation, (b) eastward current, and (c) northward current. The location of amplitude and phase estimates are shown. The 40, 100, 500, and 1000 m isobaths are shown in gray.

to determine the essential elements contributing to the observed M_2 tidal characteristics.

3.1. Horizontal Structure

[15] The CMO observations indicate that the M_2 sea level amplitude increases onshore and westward, while current amplitude increases onshore and eastward, and both have approximately constant phase (±2°) over the scale of the array (15–20 km). This is qualitatively consistent with previous observations on the New England shelf [*Moody et al.*, 1983; *Brown*, 1984]. A more complete view of the M_2 tide on the broader New England shelf is achieved by merging the results of tidal analyses performed on the CMO, CBLAST, NSFE, SEEP and Primer data with estimates of M_2 tidal amplitude and phase from *Moody et al.* [1983]. For this analysis, only currents in the upper 40 m of the water column and more than 10 m above the bottom are used. The irregularly distributed estimates of M_2 amplitude and phase are subsequently gridded (Figure 4), using a Barne's algorithm [see *Daley*, 1991] with a minimum length scale of about 50 km. The latter compares to the decorrelation length scale for M_2 current amplitude in this region which is about 70 km (estimated as the first zero crossing of the radial correlation function).

[16] The M_2 sea level elevation amplitude decreases toward the northeast, from an approximately shelf-wide 44 cm at 71.25°W to about 34 cm over the Nantucket shoals, and elevation phase increases slightly from −10°G in the southwest to 0°G on the Nantucket shoals (Figure 4). M_2 elevation phase changes rapidly over the Nantucket shoals from 0°G on the southwestern side of the bank to about 60°G on the northeastern (Gulf of Maine) side [*Moody et al.*, 1983]. The M_2 tidal current amplitudes (eastward and northward) increase strongly from southwest to northeast over the New England shelf, and phase is roughly constant with eastward and northward components about 90°G out of phase (Figure 4). M_2 tidal current amplitudes increase from only a few cm s^{-1} at about 40°N, 71°W to more than 30 cm s^{-1} over the Nantucket shoals.

[17] Horizontal structure of the M_2 tide is further examined through the depth-integrated continuity equation

$$-i\omega\eta + (hu)_x + (hv)_y = 0, \tag{3}$$

where u, v have been assumed to be barotropic. The amplitude of both eastward and northward M_2 transport increases strongly along-shelf toward the east (transport is estimated by multiplying the in situ estimates of M_2 tidal current amplitude by water depth) and phase varies about ± 20°G over the entire shelf (Figures 5a and 5b). Transport gradients are estimated via linear fit versus position between 70.50°W and 70.25°W. Eastward transport divergence, $(8.7 \pm 2.2) \times 10^{-5}$ m s^{-1}, is much larger than northward transport divergence, $(-3.4 \pm 7.7) \times 10^{-5}$ m s^{-1}.

[18] Ignoring the small horizontal variations in η and assuming the small northward transport divergence is constant over this region, equation (3) can be integrated eastward to yield

$$\left[i\omega\eta - (hv)_y\right]x = uh, \tag{4}$$

where η = 40 cm is the average M_2 sea surface height amplitude. The strong M_2 eastward transport divergence over the New England shelf is mostly balanced by the change in sea surface elevation, but including the relatively small northward transport divergence appears to close the balance (Figure 5c). The slope $i\omega\eta - (hv)_y$ = 8.9×10^{-5} m s^{-1} is nearly identical to the estimate of eastward transport divergence.

[19] The horizontal structure of M_2 sea level and currents, and the apparent depth-averaged momentum and continuity balances demonstrate the complexity of the M_2 tide on the New England shelf. The importance of the pressure gradient in the depth-averaged along-isobath momentum balance and the ellipticity of the depth-averaged M_2 tidal currents indicate that simple plane wave solutions are inadequate and that curvature of the sea surface height field is impor-

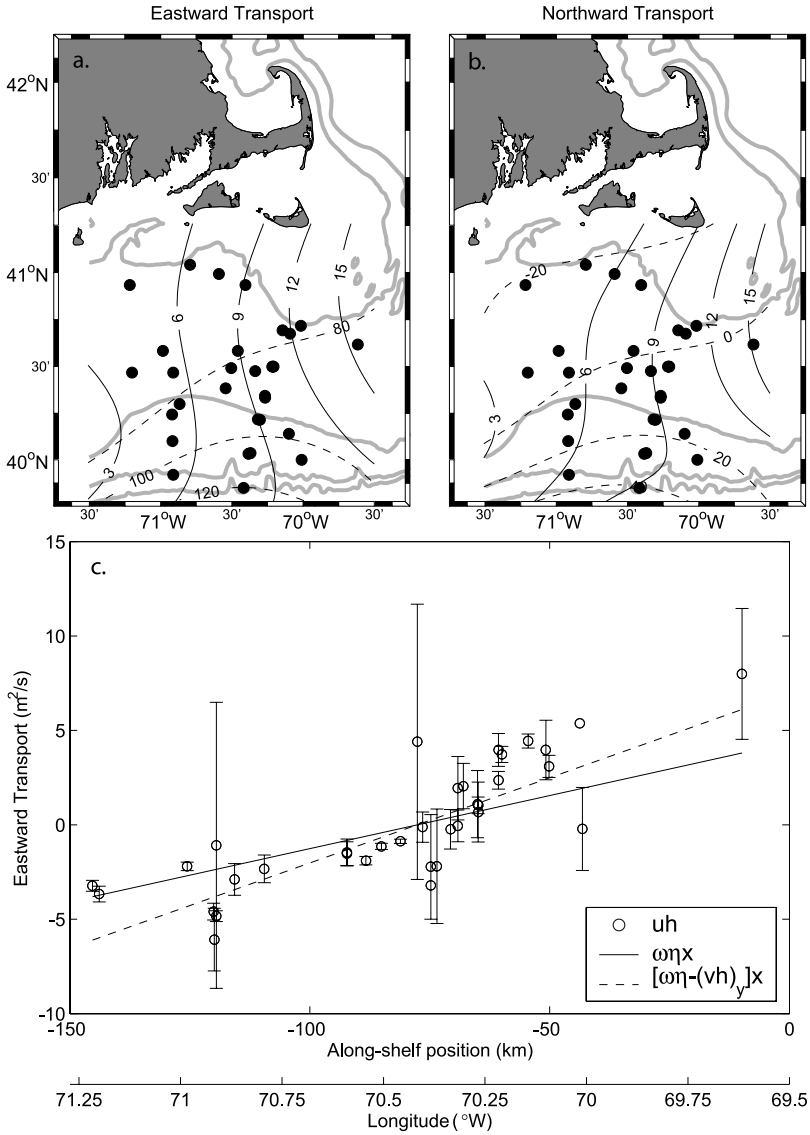

Figure 5. Maps of M_2 amplitude (solid line) and phase (dashed line) over the New England shelf for (a) eastward (uh) and (b) northward transport (vh) in $m^2\ s^{-1}$. The location of amplitude and phase estimates are shown. The 40, 100, 500, and 1000 m isobaths are shown in gray. (c) East-west variation of M_2 eastward transport and the approximations to the remainder of the integrated continuity balance, time-dependent sea surface height change, $\omega\eta x$ (solid line), and the difference between sea surface height change and northward transport divergence, $[\omega\eta - (vh)_y]x$ (dashed line).

tant. Isolines of M_2 sea level elevation and current amplitude are approximately parallel to the Nantucket shoals, and M_2 tidal current phase is approximately perpendicular. Current ellipses for the depth-averaged M_2 tidal currents are approximately perpendicular to the shoals. As noted previously, three factors may contribute to the tidal characteristics in this region: the transition between the resonant Gulf of Maine to the northeast and the MAB shelf to the west; the local bathymetry, notably the narrowing of the shelf at the Nantucket shoals; and the enhanced drag over the Nantucket shoals.

3.2. Vertical Structure

[20] Focusing on the dominant M_2 tidal constituent, the tidal ellipse parameters are nearly constant between the surface and ~20 meters above bottom (mab) and within a few percent of depth-averaged values (Figure 6). Major axes away from the bottom range from 8–12 cm s^{-1}, increasing offshore. Below 10 mab, major axis amplitudes decrease rapidly toward the bottom. Orientation ranges from about 50°–60°T, increasing slightly near the bottom. Ellipticity is approximately constant (−0.9) throughout the water column. Between 20 mab (the height of maximum amplitude) and about 2 mab, phase decreases about 20°G (currents closer to the bottom lead by ~36 min). Below 2 mab, phase and orientation increase sharply.

[21] The observed vertical structure in the M_2 characteristics is consistent with a barotropic tide and the affects of stress in the bottom boundary layer. Baroclinic tidal variability could also contribute to the vertical structure, though,

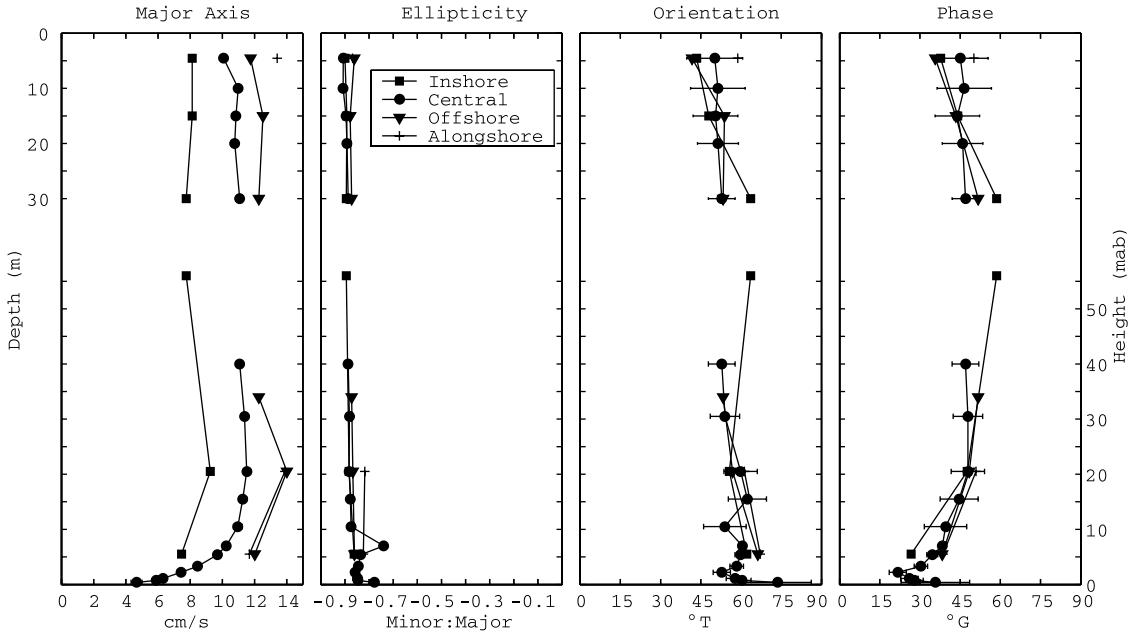

Figure 6. M_2 tidal ellipse parameters for the currents at the inshore, central, alongshore, and offshore sites: (a) major axes (cm s^{-1}), (b) ratio of minor to major axes, (c) orientation of ellipse (°T), and (d) Greenwich phase (°G). Parameters for current meters at 30 m depth or shallower are plotted versus depth, while parameters for current meters 30 m and deeper are plotted versus height above the bottom. Symbols connected with a dashed line represent results from the same current meter. The central site includes velocimeters on a bottom tripod. The 95% confidence intervals included for the central site and for other sites were similar.

if a significant portion of the baroclinic tide had a relatively constant phase over the full deployment. The mean bottom mixed layer height estimated from density observations as per *Lentz and Trowbridge* [1991] is about 10 m. The mean bottom mixed layer height corresponds partially to the depth range over which M_2 phase and amplitude are changing rapidly, a vertical structure consistent with a tidally driven boundary layer. Also, tidal variability constitutes ~26% of the total observed near-bottom stress variance with the M_2 constituent largest by approximately a factor of 2 (major axis of 0.013 ± 0.001 Pa, ellipticity of −0.78, orientation of 80° ± 9°T and phase of 58° ± 10°G).

[22] To examine whether the observed vertical structure is due to near-bottom stress, the vertical structure of the dominant terms in the horizontal momentum balance are estimated. The horizontal momentum balance is nearly identical to the depth average balance between the surface and about 20 mab. However, the local acceleration, Coriolis and pressure gradient terms do not balance near the bottom, where the local acceleration and Coriolis terms decrease rapidly. As mentioned before, the M_2 pressure gradient is essentially barotropic, indicating the baroclinic pressure gradient is not contributing to the tidal characteristics estimated over the full record.

[23] To determine whether the vertical structure near the bottom is caused by stress, the terms in the depth-integrated horizontal momentum balance relative to 10.5 mab (where stress is assumed to be zero) are computed from the BASS current observations:

$$-\int_z^{10.5} \rho_0 \left[(\mathbf{u}-\mathbf{u_0})_t + f\hat{k}\times(\mathbf{u}-\mathbf{u_0}) \right] dz' = \tau(z), \qquad (5)$$

where $\mathbf{u}_0$ is the current at 10.5 mab and the left hand side of equation (5) is referred to as the momentum deficit. The momentum deficit profile, computed from the current observations, is compared to the profile of the covariance estimates of stress. Stress profiles are also calculated using a one-dimensional, barotropic tidal model with a linear-constant eddy viscosity profile [e.g., *Lentz*, 1994; *Werner et al.*, 2003]. The eddy viscosity profile is $A_v = \kappa u_* z$ for $z < \delta/20$ and $A_v = \kappa u_* \delta/20$ for $z >= \delta/20$, where $\kappa = 0.4$ is von Karman's constant, $u_* = \sqrt{\tau_b/\rho_0}$ is the shear velocity (estimated from bottom stress) and $\delta = \kappa u_*/(\omega - f)$ is the neutral boundary layer height. The velocity profile and bottom stress are solved for iteratively, assuming a quadratic drag law, where the quadratic drag coefficient, $C_d = 1.7 \times 10^{-3}$ is determined from the CMO observations of near bottom velocity and the covariance estimates of bottom stress. The model uses 100 grid points over the 70 m water depth, with logarithmic spacing near the boundaries. Near-bottom stress is then estimated from the model velocity profile, $\boldsymbol{\tau} = A_v \mathbf{u_z}$.

[24] The major axes of the integrated momentum deficit compare very closely to the direct covariance observations of near bottom stress and modeled stress profile (Figure 7), increasing at a similar rate toward the bottom. The vertical structure exhibited by the minor axes agree well, and the values of the modeled and observed stress profiles agree, but the integrated momentum deficit is offset by about 0.05 Pa. The agreement in phase and orientation is poor, although there are similarities in the vertical structure of the observed and modeled stresses. Discrepancies in the momentum deficit are potentially due to imbalances caused by errors in the estimation of pressure gradients.

The overall comparison, however, strongly supports the hypothesis that stress is the source of near bottom structure in the M_2 tidal currents. This is notable, also, because stress in this region of the New England shelf (known as the "mud patch") is weaker than other regions by almost an order of magnitude [*Shearman and Lentz*, 2003].

4. Baroclinic Tidal Variability

[25] Baroclinic tides are a less predictable component of variability over the continental shelf. They are influenced by a variety of factors, but the most important are stratification and forcing (i.e., the barotropic tide). During CMO, stratification varies on timescales ranging from a few days to seasonal (Figure 8). Owing to this variability, the structure, phase and amplitude of baroclinic tides are potentially highly variable. Some previous observations exist demonstrating low-mode baroclinic tidal variability and higher-frequency (approaching N) internal solitons generated on tidal intervals over the New England shelf [e.g., *Colosi et al.*, 2001; J. A. MacKinnon and M. C. Gregg, Mixing on the late summer New England shelf: Solibores and stratification, submitted to *Journal of Geophysical Research*, 2001]. The low-mode internal waves are thought to be generated by the semidiurnal barotropic tide near the shelfbreak and propagate onshore, developing the higher-frequency solitons through nonlinear processes.

[26] During CMO, similar bore-like features are observed along the pycnocline in the fall (Figure 9a) and spring. During the winter, stratification is stronger near the bottom (Figure 8) due to the presence of the foot of the shelfbreak front [*Lentz et al.*, 2003], and bore-like structures are found at depth (Figure 9b). At semidiurnal frequencies, rms isotherm displacements are less than 1 m, and maximum isotherm displacements are on the order of 3–4 m. Isotherm displacements associated with the high-frequency (24–96 cpd) solitons are about 2 m rms and 10 m maximum. Displacements are about the same in winter as fall and spring. The temperature variability (Figure 9) suggests that the phasing of the internal tide is highly variable, but frequently the leading edge of more dramatic internal bores coincides with the peak M_2 onshore barotropic flow (e.g., 1400 UT 31 August 1996 and 1200 UT 19 January 1997).

[27] For the CMO observations, complex empirical orthogonal functions (CEOFs) are used to characterize the vertical structure of the high-passed current variability at each mooring site (Figure 10). The dominant mode is the barotropic tide, which accounts for about 70% of the total high-passed current variability. The second and third CEOFs resemble first and second baroclinic modes. CEOF 2 has one zero crossing at about 30 m, accounts for ~8% (inshore) to 30% (offshore) of the high-passed current variability, and is characterized mainly by near-inertial variability, but has a significant narrow-banded peak at the M_2 tidal frequency (Figure 11). CEOF 3 has zero crossings at about 15 and 50 m, accounts for around 5% of the high-passed variability (increasing in the off-shelf direction), and has a significant peak at the M_2 frequency, as well. It should be noted that CEOFs 2 and 3 do not necessarily represent distinct dynamical modes. Semidiurnal band variance of the CEOF 2 and 3 time series are about 10–30% of the inertial band variance, and only 2–15% of the semidiurnal variance in the barotropic mode, indicating baroclinic tides are a relatively small component of current variablity at the CMO site.

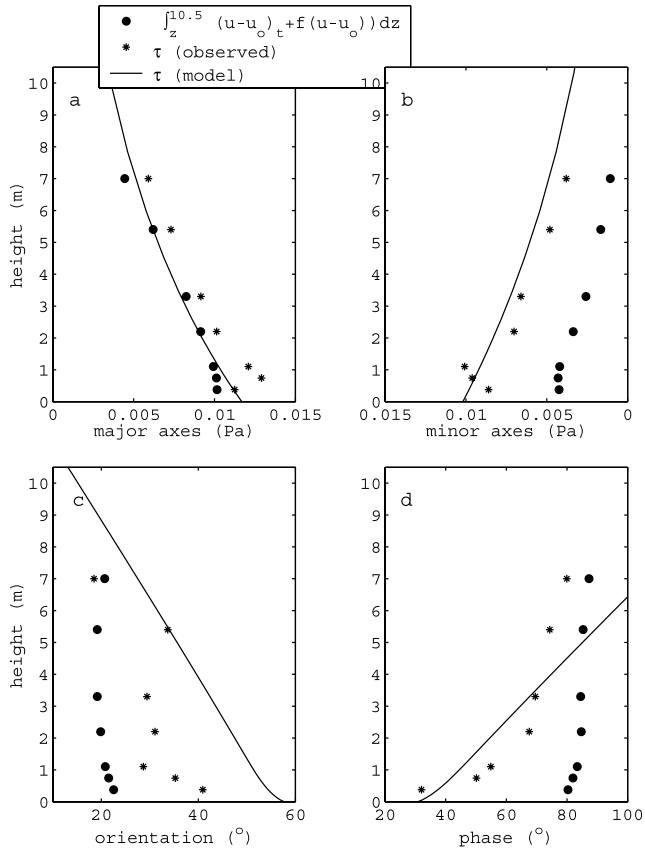

Figure 7. Profiles of the M_2 (a) major axes, (b) minor axes, (c) ellipse orientation, and (d) phase for the observed momentum deficit (circles), observed covariance stresses (asterisks), and model stresses (lines) between the bottom and 10.5 m above the bottom at the central site. The model is a one-dimensional tidal model with a linear-constant eddy viscosity profile [e.g., *Werner et al.*, 2003].

[28] The time series of the baroclinic modes (CEOFs 2 and 3) are coherent with the barotropic mode (CEOF 1) at semidiurnal frequencies (coherence of about 0.70 with 95% significance level of 0.45) with the baroclinic mode ~90° out of phase. This suggests that baroclinic tidal variability is on average phase locked to the barotropic tide. As indicated by the temperature time series, however, there is high degree of variability to the relative phasing. The time series of CEOFs 2 and 3 are also coherent across isobaths with a phase difference of about 120° between the central and offshore mooring sites, corresponding to a cross-isobath wavelength of about 7 km, which approximately matches the wavelength expected for linear internal waves with a vertical wavelength of 70 m and buoyancy frequency of 106 cpd (the CMO average).

[29] Semidiurnal band variance of the CEOF 2 time series (estimated on weekly intervals) is larger in the fall and

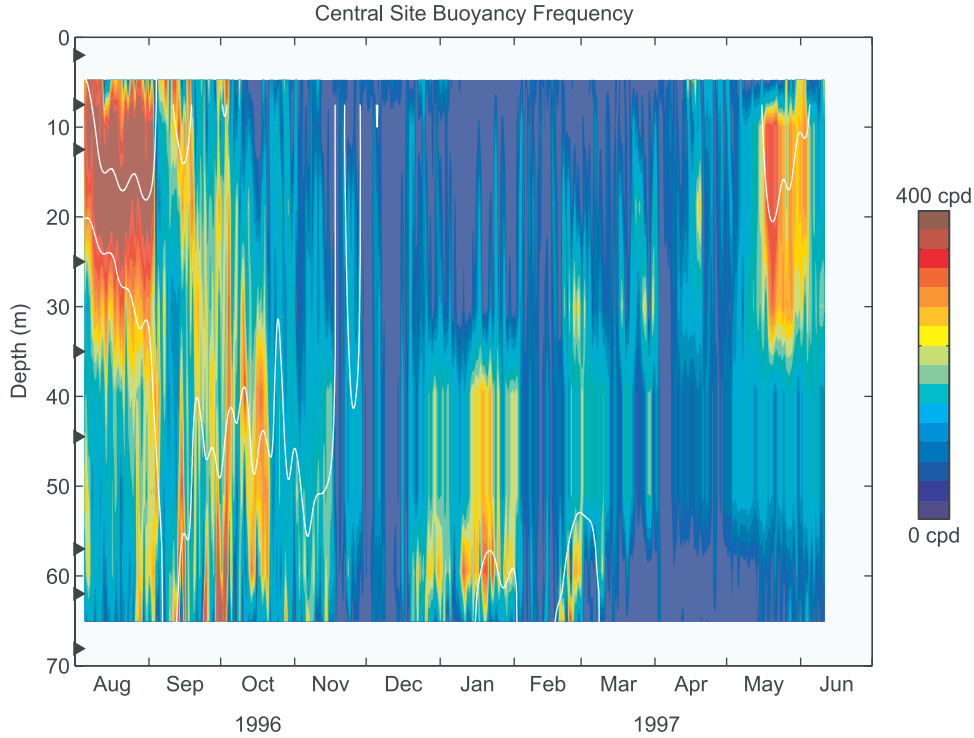

Figure 8. Buoyancy frequency N (cpd), during CMO, estimated from density observations (23.5, 24.5, and 25.5 σ_t contoured in white) at the central site.

spring than in winter (Figure 12a), following the approximate seasonal variation in stratification (Figure 8). The period of near bottom wintertime stratification, however, does not correspond to an increase in low-mode semidiurnal current variance. In addition, the harmonic tidal analysis, repeated on weekly intervals using the detided current meter data (to remove the large barotropic tidal signal), has larger M_2 cross-isobath current amplitudes (maximum of 4–5 cm s^{-1}) in the fall and spring (Figure 12b). The vertical structure is consistent with a first baroclinic mode with amplitude maxima at about 15 and 55 m, and a minimum at 30–40 m. Weeks with relatively large amplitude (Table 3) have an average upper- and lower-layer cross-isobath M_2 current amplitude of 2.7 ± 0.3 cm s^{-1} and an upper-lower phase difference of 183 ± 5°G (error estimate is standard deviation of the mean). The baroclinic M_2 tidal current ellipses are polarized across-isobath with an average orientation of 14° ± 9°T, and have an average ellipticity of −0.66 ± 0.02, which is significantly different from the ellipticity of the barotropic M_2 tide and very near f/ω, consistent with the dynamics of linear plane waves. The phase of the baroclinic tide is highly variable, and the mean value is misleading, since none of the weeks actually has a value of 42°G. However, there are examples when the upper-level cross-isobath currents are in phase with the barotropic cross-isobath currents (15°G), such as weeks 1 and 2. There are also examples when the upper-level baroclinic M_2 cross-isobath currents are in phase with the barotropic along-isobath currents (105°G), such as weeks 8, 18 and 44. This suggests that while phase locking may occur, it is not common and the phase relation may change.

[30] The dynamics of the baroclinic tide are examined through weekly estimates of the terms in the M_2 along- and cross-isobath momentum balances with the barotropic (full record) tide removed. The dominant terms are the local acceleration, Coriolis and baroclinic pressure gradient, in that order, with the magnitude of pressure gradient terms being about 30–60% of the local acceleration terms. The along- and cross-isobath pressure gradients are similar in magnitude. The M_2 local acceleration term is approximately balanced by the sum of the Coriolis and pressure gradient terms with close agreement in both phase and amplitude (Figure 13). Linear regression slopes for amplitude are 0.8 ± 0.1 and for phase are 1.0 ± 0.4 in both directions. The dynamics suggested by the apparent momentum balance are not consistent with a two-dimensional linear plane wave propagating from offshore (the along-isobath pressure gradient would be negligible in this case). Instead, the dynamics suggest a more three-dimensional structure to the internal tide, as opposed to the ellipticity values that are consistent with at two-dimensional structure.

4.1. High-Frequency Internal Solitons

[31] In addition to the low-mode baroclinic tide, high-frequency internal solitons (similar, but smaller in magnitude, to those observed by *Colosi et al.* [2001]) are observed at the CMO moored array. During the fall and spring, high-frequency internal solitons are observed in conjunction with the bore-like structures at the pycnocline depth of about 20 m (Figure 9a). During the winter, high-frequency solitons are found along the deeper pycnocline at 55 m depth (Figure 9b). During the fall and spring, internal solitons are manifested as waves of depression, while during

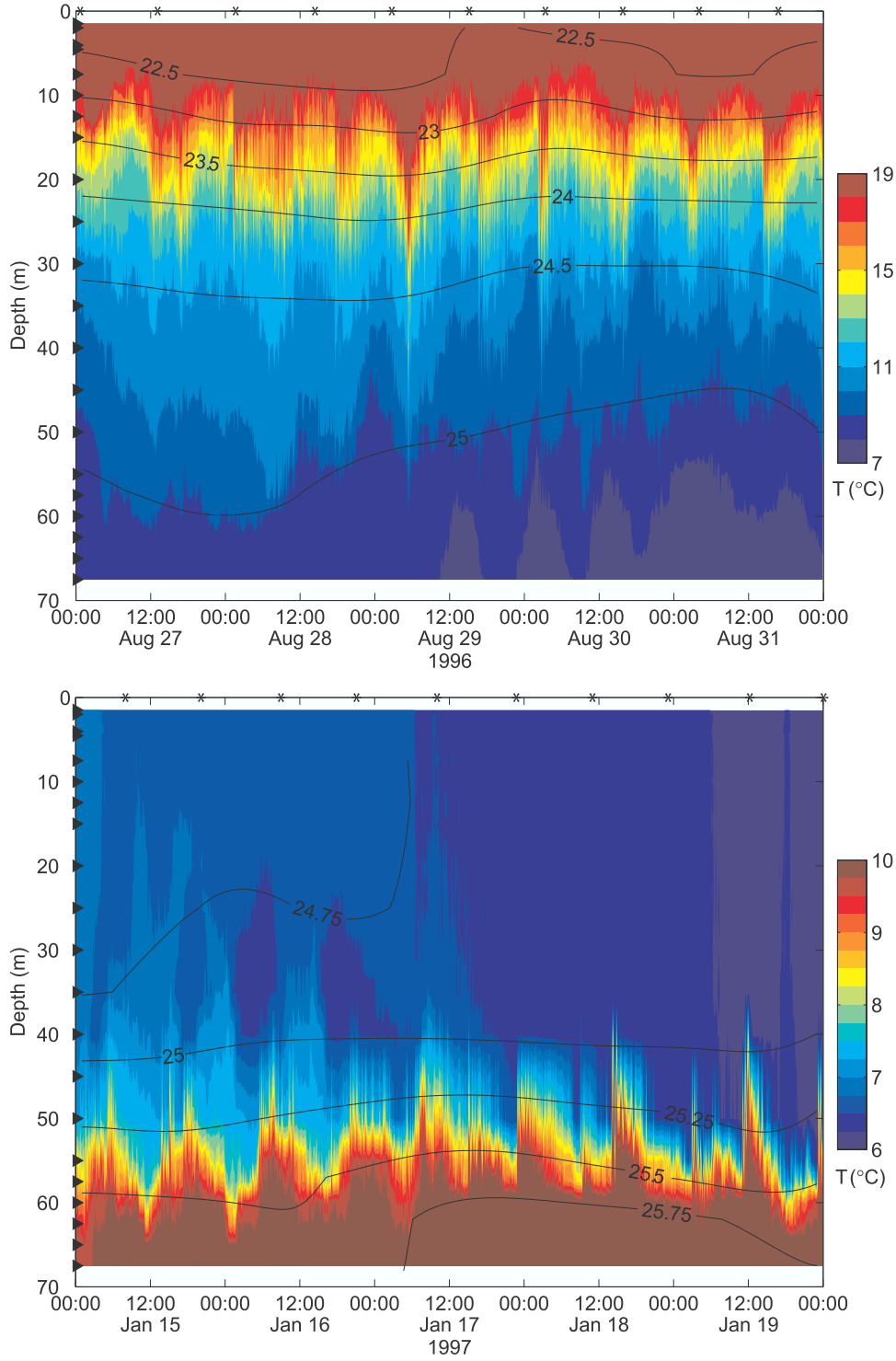

Figure 9. Raw (7.5 min) moored temperature observations and subtidal σ_t at the central site for (a) 27–31 August 1996 and (b) 15–19 January 1997. The time of peak M_2 onshore barotropic flow is indicated by an asterisk.

the winter, they appear to be waves of elevation. Although winter stratification is weaker than fall or spring, typical isotherm displacements are similar. Current variability associated with high-frequency solitons, estimated as the standard deviation of the high-passed (greater than 24 cpd) raw VMCM observations, is 0.5–2.0 cm s^{-1} (standard deviation), decreasing in the onshore direction. The intensity and vertical structure of high-frequency current variability, associated with the internal solitons, is strongly related to stratification. Depth-integrated high-frequency current variance is linearly related to depth-integrated N^2 (Figure 14) on weekly intervals with stronger variability

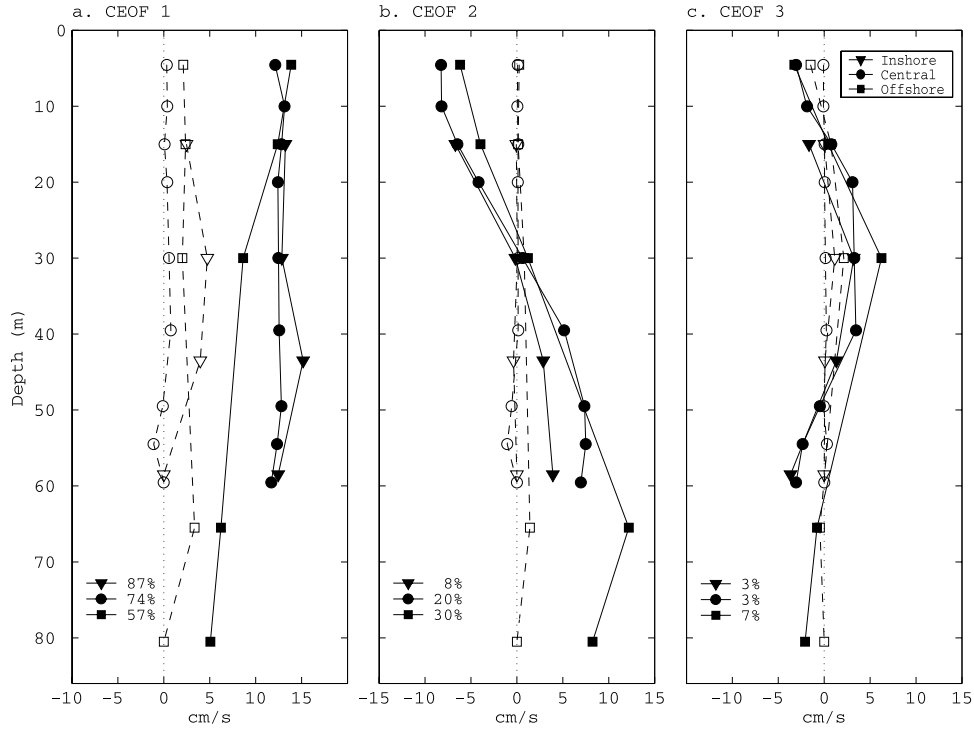

Figure 10. (a–c) The first three complex empirical orthogonal functions (CEOFs), estimated from the high-passed (>0.7 cpd)vector-measuring current meter observations at the central, inshore, and offshore sites. Percent variance for each mode is also shown. The real component is indicated by solid lines and symbols, and the imaginary component is indicated by dashed lines and open symbols.

generally during the fall. The vertical structure is tied to peak stratification with high correlation between the depth of maximum high-frequency current variability and maximum stratification (Figure 15). When the maximum stratification is less than 30 m, the depth of maximum kinetic energy is about 5 m deeper, and when maximum stratification is deeper than 35 m, the depth of maximum kinetic energy is shallower by a about 5 m. This change also corresponds approximately to

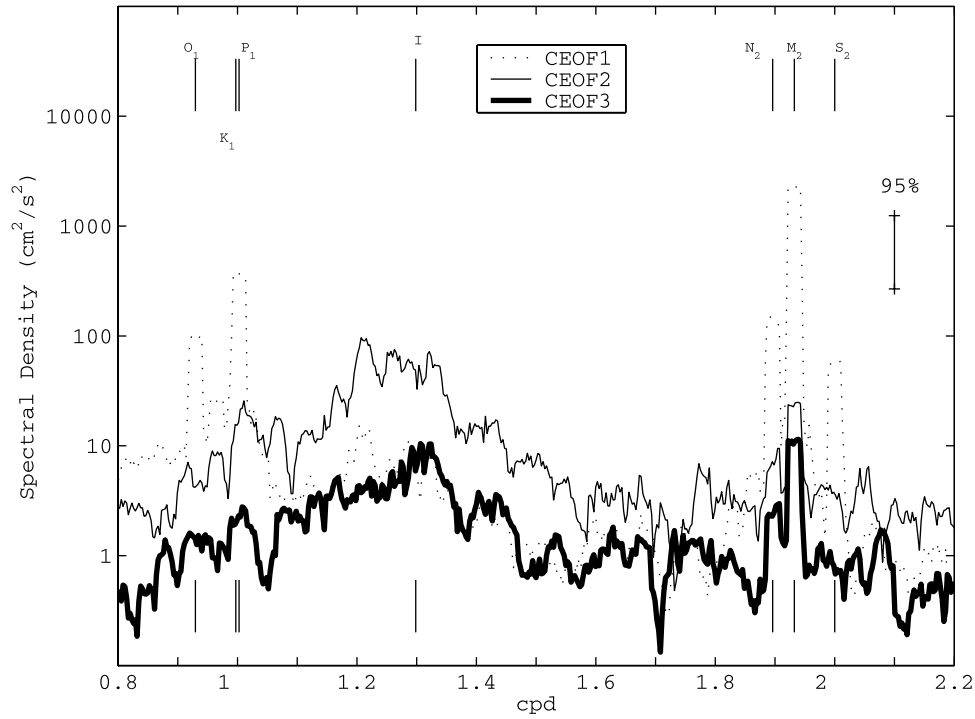

Figure 11. Spectra of the cross-isobath component of CEOFs 1, 2, and 3 at the central site.

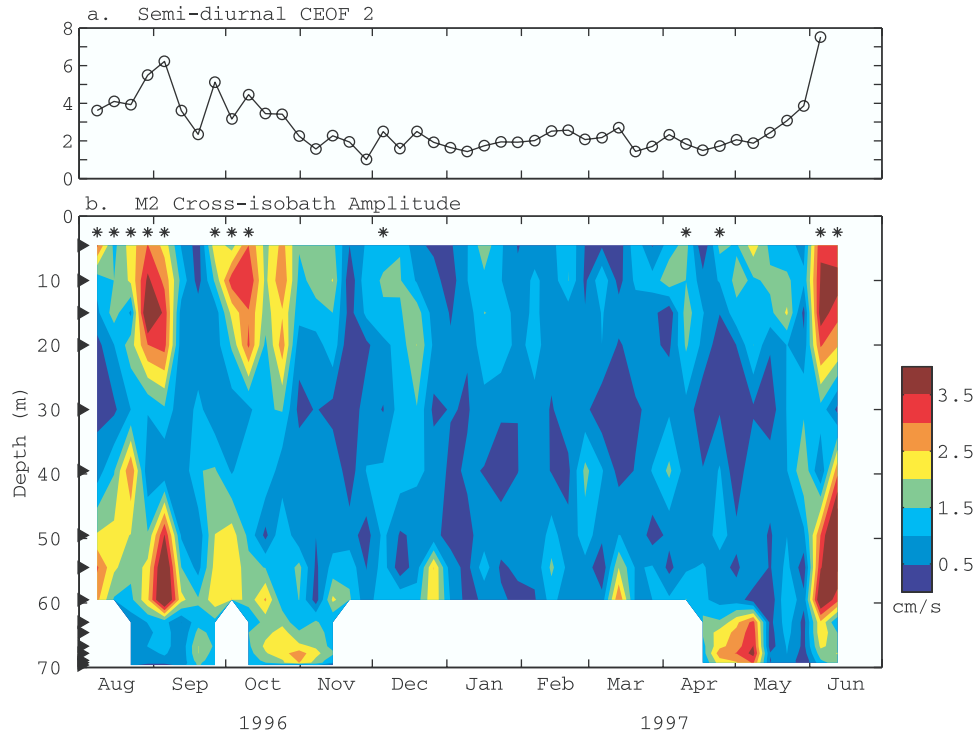

Figure 12. (a) Weekly semidiurnal variance of the CEOF 2 time series at the central site. (b) Weekly M_2 cross-isobath current amplitude from harmonic analysis of the detided currents at the central site. Large-amplitude events are identified by asterisks.

the switch from internal solitons that appear to be waves of depression to waves of elevation.

4.2. Cross-Shelf Structure

[32] Observations from the CMO moored array indicate that low-mode baroclinic tidal variability and high-frequency current variability decrease in the onshore direction. Several processes may extract energy from the low-mode baroclinic tide as it propagates onshore (e.g., the generation of internal solitons and bottom drag), and high-frequency internal solitons may also experience bottom drag and possibly dissipation due to nonlinear steepening and wave breaking.

[33] The gross cross-shelf structure of semidiurnal internal tidal current variance (or kinetic energy) and high-frequency current variance on the New England shelf is examined through the compilation of the moored, near surface current observations from several observational programs. First, current meter observations are detided using the full record harmonic analysis, then the semidiurnal band variance of the detided time series is computed. Semidiurnal baroclinic tidal current variance and high-frequency current variance decrease on shore at approximately the same rate, about -2.4×10^{-5}J m^{-1} (after multiplying by ρ_0). Interestingly, this decrease is linearly related to bottom depth inshore of the 200 m isobath (Figure 16).

[34] Dissipation along the internal wave path is certainly a possibility for the observed decrease in energy. Because high-frequency and low-mode baroclinic energy both decrease onshore, low-mode energy loss through the generation of high-frequency solitons does not appear to be the likely cause; an increase in high-frequency energy would be expected in this case. The nearly linear relation between energy and bottom depth, though, supports the idea that bottom stress may play an important role in extracting energy from baroclinic tides and internal waves.

5. Discussion and Summary

[35] Observations from the Coastal Mixing and Optics moored array have been used to characterize the three-

Table 3. Upper Water Column M_2 Ellipticity and Ellipse Orientation From Weeks With Relatively Large Amplitude Baroclinic Tidal Signals at the Central Site

Week	Ellipticity	Ellipse Orientation, °T	Cross-Isobath Amplitude,[a] cm s^{-1}	Cross-Isobath Phase,[b] °G	Phase Difference, °G
1	−0.78	24	2.1 (3.1)	23	171
2	−0.74	−8	1.5 (2.2)	19	176
3	−0.70	−2	2.3 (2.5)	−96	217
4	−0.65	−12	4.4 (2.4)	167	177
5	−0.70	72	3.3 (2.5)	175	177
8	−0.68	80	2.3 (2.3)	125	166
9	−0.53	−13	3.3 (2.5)	−76	190
10	−0.62	8	3.1 (1.7)	−35	207
18	−0.47	12	1.5 (1.4)	106	157
36	−0.72	−26	1.8 (1.5)	−51	205
38	−0.56	35	1.7 (1.3)	153	182
44	−0.63	−7	3.8 (4.2)	90	187
45	−0.81	23	3.8 (4.8)	−52	171
Mean	**−0.66 ± 0.02**	**14 ± 9**	**2.7 (2.7) ± 0.3**	**42 ± 27**	**183 ± 5**

[a] M_2 amplitude of the upper-level (lower-level) cross-isobath currents.
[b] M_2 phase of the upper cross-isobath currents and upper-lower phase difference.

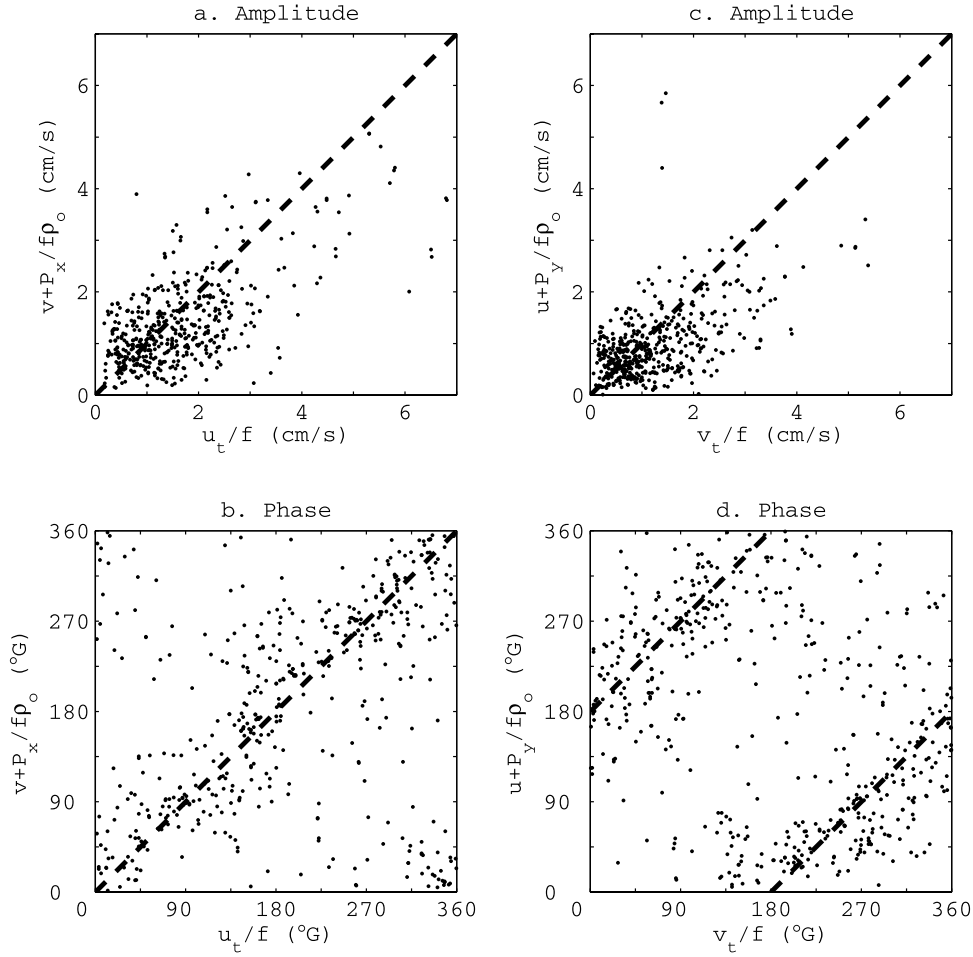

Figure 13. Comparison of (top) amplitude and (bottom) phase for the local acceleration and the Coriolis plus pressure gradient terms in the baroclinic M_2 tidal (a–b) along-isobath and (c–d) cross-isobath momentum balance. Dashed lines have a slope of 1.

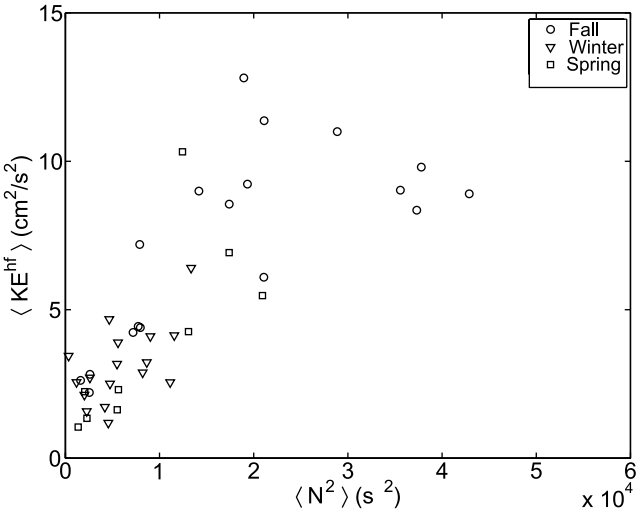

Figure 14. Weekly estimates of depth-averaged N^2 at the central site versus weekly depth-averaged estimates of high-frequency kinetic energy from current variance over the 24–96 cpd band.

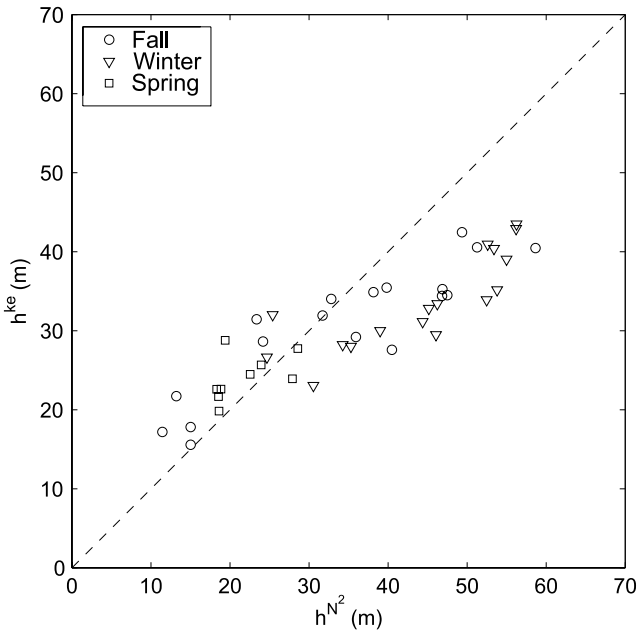

Figure 15. Comparison of depth of maximum stratification (N^2) and depth of maximum high-frequency kinetic energy on weekly intervals.

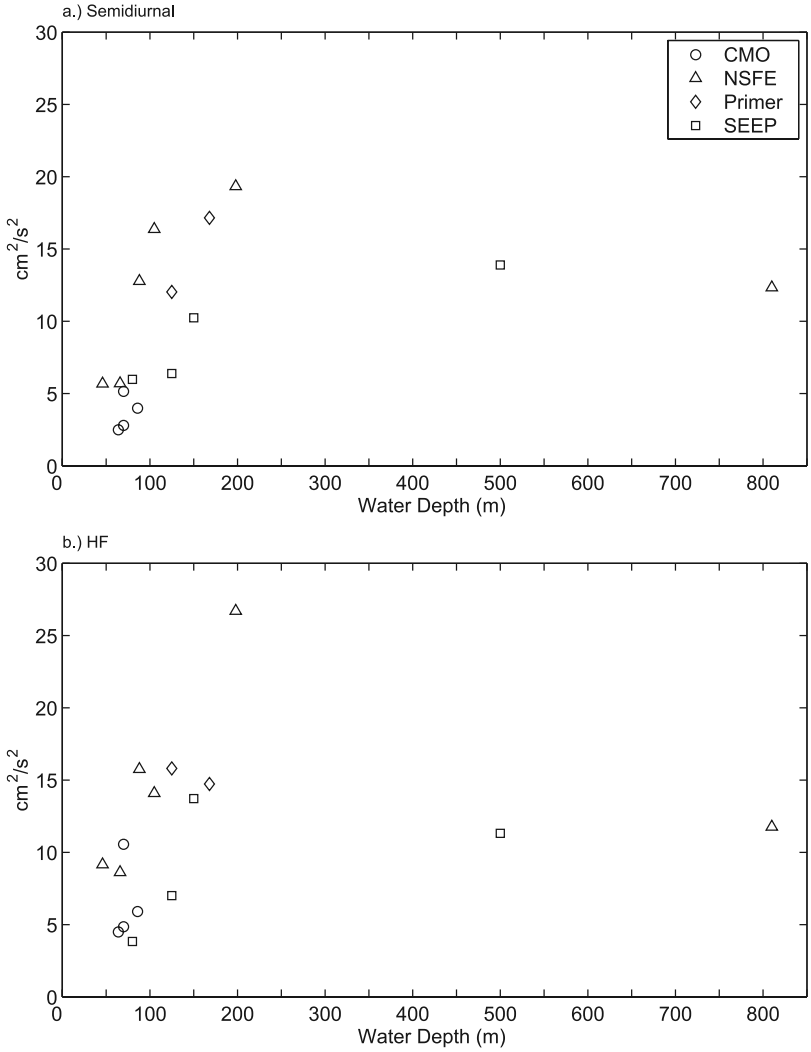

Figure 16. (a) Semidiurnal and (b) high-frequency detided current variance (above 40 m), representing baroclinic current variance, versus water depth. Current variance decreases approximately linearly with bottom depth.

dimensional structure, temporal variability and dynamics of barotropic and baroclinic tidal variability on the New England shelf. Although the New England shelf is relative minimum in tidal amplitude along the MAB, the barotropic M_2 tide constitutes a large fraction of the total current and sea level variance at the CMO site. The dynamics of the M_2 tide on the New England shelf are more complex than either the nearby New Jersey shelf or the Gulf of Maine and Georges Bank. The M_2 along-isobath pressure gradient is as large as the cross-isobath pressure gradient, and tidal current ellipses are only weakly polarized. The implication for tidal dynamics is that the M_2 tide on the New England shelf cannot be modeled as a single standing or progressive planar wave.

[36] The source of the along-isobath pressure gradient is potentially related to the bathymetric irregularity caused by the Nantucket shoals, which is the location of a strong local minimum in M_2 tidal elevation and maximum in tidal currents. The arrangement of M_2 phase (perpendicular) and amplitude (parallel) suggests that the Nantucket shoals exert some influence over tidal variability on the New England shelf. For instance, an along-isobath M_2 pressure gradient could be the result of bathymetric affects associated with shoals (e.g., sudden narrowing of the shelf toward the east). Increased dissipation, associated with strong tidal currents, over the shoals might also affect the along-isobath pressure gradients. There is clear motivation in these observations for a modeling study to improve our understanding of the M_2 tidal characteristics on the New England shelf.

[37] The vertical structure of the barotropic M_2 currents near the bottom is caused by stress in the tidally driven bottom boundary layer, even though bottom stress at the CMO site is unusually weak compared to other shelves. Estimates of the vertically integrated M_2 momentum deficit match closely in amplitude (but not phase) the direct covariance estimates of stress in the bottom 7 m.

[38] Low-mode baroclinic tides are weak at the CMO site over the New England shelf with maximum amplitudes of about 4 cm s^{-1}. The vertical structure is consistent with a first baroclinic mode, and baroclinic M_2 tidal ellipses are oriented across-isobath and have an ellipticity that approximately matches f/ω, suggesting linear plane wave

dynamics. Direct estimates of the baroclinic M_2 tidal momentum balance show that the dynamics are linear (local acceleration, Coriolis and pressure gradient terms dominate), but along-isobath pressure gradients are as large as the cross-isobath gradient. Thus if the baroclinic tide is propagating across-isobath as suggested by previous observations and the CMO estimates of ellipticity, the low-mode baroclinic tide likely has an important three-dimensional structure. In addition, high-frequency internal solitons, generated on semidiurnal intervals, are found following the pycnocline. During the winter, the stratification is strongest at depth and high-frequency internal solitons are found manifested as waves of elevation as opposed to waves of depression that are typical for fall or spring. In general, the baroclinic tidal and high-frequency internal current variance is strongly related to stratification, and decreases across the shelf. Dissipation due to bottom stress may play an important role given the strong linear relationship between bottom depth and baroclinic kinetic energy.

[39] Barotropic and baroclinic tidal variability on the New England shelf is complex in structure and dynamics. This study has provided some details on that structure and dynamics, however, important problems remain, such as the mechanism for the dissipation of the internal tides and understanding more fully the affect of the Nantucket shoals on the regional tidal dynamics.

[40] **Acknowledgments.** We thank N. Galbraith, W. Ostrom, R. Payne, R. Trask, G. Tupper, J. Ware, and B. Way of the WHOI Upper Ocean Processes Group and the WHOI Rigging Shop under the direction of D. Simoneau, with assistance from M. Baumgartner, C. Marquette, M. Martin, N. McPhee, E. Terray, and S. Worrilow, for the design, deployment, and recovery of the moored array, for the preparation of the instruments, and for the processing of the data. Also, we are grateful for the contributions of R. Beardsley and J. Lerczak. Funding for the CMO experiment and subsequent analysis was provided by the Office of Naval Research under grants N00014-95-1-0339 and N00014-01-1-0140.

References

Aikman, F., III, H. W. Ou, and R. W. Houghton (1988), Current variability across the New England continental shelf-break and slope, *Cont. Shelf Res.*, *8*, 625–651.

Beardsley, R. C. (1987), A comparison of the vector-averaging current meter and New Edgerton, Germeshausen, and Grier, Inc., vector-measuring current meter on a surface mooring in Coastal Ocean Dynamics Experiment 1, *J. Geophys. Res.*, *92*, 1845–1860.

Beardsley, R. C., H. Mofjeld, M. Wimbush, C. N. Flagg, and J. J. Vermersch Jr. (1977), Ocean tides and weather-induced bottom pressure fluctuations in the Middle-Atlantic Bight, *J. Geophys. Res.*, *82*, 3175–3182.

Beardsley, R. C., D. C. Chapman, K. H. Brink, S. R. Ramp, and R. Schlitz (1985), The Nantucket Shoals Flux Experiment (NSFE79). Part I: A basic description of the current and temperature variability, *J. Phys. Oceanogr.*, *15*, 713–748.

Beardsley, R. C., J. Candela, R. Limeburner, W. R. Geyer, S. J. Lentz, B. M. Castro, D. Cacchione, and N. Carneiro (1995), The M_2 tide on the Amazon shelf, *J. Geophys. Res.*, *100*, 2283–2319.

Brown, W. S. (1984), A comparison of Georges Bank, Gulf of Maine, and New England shelf tidal dynamics, *J. Phys. Oceanogr.*, *14*, 145–167.

Clarke, A. J. (1991), The dynamics of barotropic tides over the continental shelf and slope (review), in *Tidal Hydrodynamics*, edited by B. B. Parker, pp. 79–108, John Wiley, Hoboken, N. J.

Colosi, J. A., R. C. Beardsley, J. F. Lynch, G. Gawarkiewicz, C.-S. Chiu, and A. Scotti (2001), Observations of nonlinear internal waves on the outer New England continental shelf during the summer Shelfbreak Primer study, *J. Geophys. Res.*, *106*, 9587–9601.

Daifuku, P. R., and R. C. Beardsley (1983), The K_1 tide on the continental shelf from Nova Scotia to Cape Hatteras, *J. Phys. Oceanogr.*, *13*, 3–17.

Daley, R. (1991), *Atmospheric Data Analysis*, Cambridge Univ. Press, New York.

Dickey, T. D., and A. J. Williams III (2001), Interdisciplinary ocean process studies on the New England shelf, *J. Geophys. Res.*, *106*, 9427–9434.

Foreman, M. G. (1977), Manual for tidal heights analysis and prediction, *Pac. Mar. Sci. Rep. 77-10*, Inst. of Ocean Sci., Victoria, B. C., Canada.

Foreman, M. G. (1978), Manual for tidal currents analysis and prediction, *Pac. Mar. Sci. Rep. 78-6*, Inst. of Ocean Sci., Victoria, B. C., Canada.

Fratantoni, P. S., and R. S. Pickart (2003), Variability of the shelf break jet in the Middle Atlantic Bight: Internally or externally forced?, *J. Geophys. Res.*, *108*(C5), 3166, doi:10.1029/2002JC001326.

Galbraith, N., A. Plueddemann, S. Lentz, S. Anderson, M. Baumgartner, and J. Edson (1999), Coastal Mixing and Optics experiment moored array data report, *Tech. Rep. WHOI-99-15*, Woods Hole Oceanogr. Inst., Woods Hole, Mass.

Gawarkiewicz, G., K. H. Brink, F. Bahr, R. C. Beardsley, M. Caruso, J. F. Lynch, and C.-S. Chiu (2004), A large-amplitude meander of the shelf-break front during summer south of New England: Observations from the Shelfbreak PRIMER experiment, *J. Geophys. Res.*, *109*, C03006, doi:10.1029/2002JC001468.

Houghton, R. W., F. Aikman III, and H. W. Ou (1988), Shelf-slope frontal structure and cross-shelf exchange at the New England shelf-break, *Cont. Shelf Res.*, *8*, 687–710.

Lentz, S. J. (1994), Current dynamics over the northern California inner shelf, *J. Phys. Oceanogr.*, *24*, 2461–2478.

Lentz, S. J., and J. H. Trowbridge (1991), The bottom boundary layer over the northern California shelf, *J. Phys. Oceanogr.*, *21*, 1186–1201.

Lentz, S. J., M. Carr, and T. H. C. Herbers (2001), Barotropic tides on the North Carolina shelf, *J. Phys. Oceanogr.*, *31*, 1843–1859.

Lentz, S. J., R. K. Shearman, S. Anderson, A. J. Plueddemann, and J. Edson (2003), Evolution of stratification over the New England shelf during the Coastal Mixing and Optics study, August 1996–June 1997, *J. Geophys. Res.*, *108*(C1), 3008, doi:10.1029/2001JC001121.

Linder, C. A., and G. Gawarkiewicz (1998), A climatology of the shelf-break front in the Middle Atlantic Bight, *J. Geophys. Res.*, *103*, 18,405–18,423.

Moody, J. A., et al. (1983), Atlas of tidal elevation and current observations on the northeast American continental shelf and slope, *U.S. Geol. Surv. Bull.*, *1161*, 1–122.

Pawlowicz, R., R. Beardsley, and S. Lentz (2002), Harmonic analysis including error estimates in MATLAB using T-TIDE, *Comput. Geosci.*, *28*, 929–937.

Shaw, W. J., J. H. Trowbridge, and A. J. Williams III (2001), Budgets of turbulent kinetic energy and scalar variance in the continental shelf bottom boundary layer, *J. Geophys. Res.*, *106*, 9551–9564.

Shearman, R. K., and S. J. Lentz (2003), Dynamics of mean and subtidal flow on the New England shelf, *J. Geophys. Res.*, *108*(C8), 3281, doi:10.1029/2002JC001417.

Werner, S. R., R. C. Beardsley, S. J. Lentz, D. L. Hebert, and N. S. Oakey (2003), Observations and modeling of the tidal bottom boundary layer on the southern flank of Georges Bank, *J. Geophys. Res.*, *108*(C11), 8005, doi:10.1029/2001JC001271.

Williams, A. J., III, J. S. Tochko, R. L. Koehler, W. D. Grant, T. F. Gross, and C. V. R. Dunn (1987), Measurement of turbulence in the oceanic bottom boundary layer with an acoustic current meter array, *J. Atmos. Oceanic Technol.*, *4*, 312–327.

S. J. Lentz and R. K. Shearman, Department of Physical Oceanography, MS 21, Woods Hole Oceanographic Institution, 360 Woods Hole Road, Woods Hole, MA 02543, USA. (slentz@whoi.edu; kshearman@whoi.edu)